Spin assignment and statistical properties of neutron resonances from ^{161,163}Dy(n,γ) and ^{167}Er(n,γ) measured at the DANCE facility

I. Knapová,[1,*] S. Valenta,[1,†] B. Baramsai,[2,‡] T. A. Bredeweg,[3] A. Couture,[3] C. Fry,[3] M. Jandel,[3,§] J. Kroll,[3,‖] M. Krtička,[1] G. E. Mitchell,[2,¶] J. M. O'Donnell,[3] C. J. Prokop,[3] G. Rusev,[3] and J. L. Ullmann[3]

[1]*Faculty of Mathematics and Physics, Charles University, Prague, Czech Republic*
[2]*North Carolina State University, Raleigh, North Carolina 27695, USA*
and Triangle Universities Nuclear Laboratory, Durham, North Carolina 27708, USA
[3]*Los Alamos National Laboratory, P.O. Box 1663, Los Alamos, New Mexico 87545, USA*

(Received 3 May 2022; revised 16 June 2022; accepted 15 July 2022; published 19 September 2022)

Background: Average resonance spacing D_0 and spin dependence of nuclear level density (NLD) are essential quantities in nuclear physics, especially important for calculations of nuclear reactions and the normalization of NLD models.
Purpose: Neutron resonances with different spins in odd-mass targets can form close doublets that are often difficult to resolve. These doublets are not corrected for when accounting for subthreshold resonances during D_0 determination. Moreover, different literature sources disagree on the isotopic assignment of some resonances.
Methods: The γ rays following radiative neutron capture on ^{161,163}Dy and ^{167}Er were measured with the highly segmented γ-ray calorimeter Detector for Advanced Neutron Capture Experiments (DANCE) at the Los Alamos Neutron Science Center. The analysis of spectra using the γ-multiplicity-based spin assignment method allows checking for the presence of the above-mentioned doublets. The calorimetric sensitivity provides unambiguous isotopic assignment.
Results: We were able to assign spin to tens of resonances as well as to identify new ones in all three isotopes. Some isotope assignments from the literature were corrected. Detailed analysis of the number of unobserved resonances, assuming that the resonance positions obey predictions of the Gaussian orthogonal ensemble and reduced neutron widths Porter-Thomas fluctuations, allowed determination of D_0 with an uncertainty of a few percent, $D_0 = 2.15(5)$, 6.39(24), and 3.86(12) eV for ^{161,163}Dy and ^{167}Er, respectively. Thanks to the spin assignment, the spacings for the resonances with the two spins formed in s-wave neutron capture, D_0^- and D_0^+, were determined. Their ratio was compared to different NLD models.
Conclusions: Our deduced D_0 for ^{163}Dy is lower than any ^{163}Dy value found in the literature. Good consistency was found with some literature values for ^{161}Dy and ^{167}Er. The ratios D_0^-/D_0^+ are consistent with several models available in the literature, but in a clear contradiction with a few microscopic NLD models.

DOI: 10.1103/PhysRevC.106.034607

I. INTRODUCTION

Experimental studies of neutron resonances play a very important role in nuclear physics. The density of resonances with different spins is of great interest as it is a key quantity in calculations of cross sections in many areas, including nuclear astrophysics [1,2], stockpile stewardship, and advanced fuel cycle calculations [3]. This density also serves as an anchor point for the adjustment of the nuclear level density (NLD) models. Common challenges in neutron resonance spectroscopy are limited ability to observe weak resonances, resolve close doublets, and determine resonance spin, especially on targets with nonzero spin. These imply difficulties in observation of a complete and at the same time pure sequence of resonances with a given spin and parity. The correct spin assignment allows not only correct NLD determination but serves as an important check of its spin dependence.

In the following, we restrict ourselves to nuclei for which the conditions, e.g., high level density, practically prevent observation of resonances with orbital momentum $\ell > 0$. If only one s-wave resonance spin is allowed, which is the case for zero-spin targets, the repulsion of individual levels with the same spin and parity prevents the presence of very small spacings. The situation is, however, different for nonzero spin targets as no repulsion is expected among levels with different spins. Even facilities with excellent neutron energy resolution thus reach a limit on doublet resolving power. The presence of unresolved doublets can then lead to inappropriate average s-wave resonance spacing D_0 deduced from experimental data. This is the case even if data are corrected for weak resonances

*knapova@ipnp.mff.cuni.cz
†valenta@ipnp.mff.cuni.cz
‡Present address: Vantage Partners, NASA Glenn Research Center, Brook Park, OH 44142, USA.
§Present address: Department of Physics and Applied Physics, University of Massachusetts Lowell, Lowell, MA 01854, USA.
‖Present address: Institute of Physics, Academy of Sciences of the Czech Republic, Prague, Czech Republic.
¶Deceased.

that escape detection due to a strong Porter-Thomas fluctuation of reduced neutron widths $\Gamma_n^0 = \Gamma_n/\sqrt{E/1\,\mathrm{eV}}$.

In this paper, we show an application of a multiplicity-based method [4] on the γ-ray spectra following the neutron capture in three rare-earth isotopes, ^{161,3}Dy and ^{167}Er, measured with Detector for Advanced Neutron Capture Experiments (DANCE), a highly segmented highly-efficient γ calorimeter located at Los Alamos Neutron Science Center (LANSCE) of Los Alamos National Laboratory (LANL). The main advantage of the method is its capability of revealing extremely close resonance doublets at low neutron energies, where the neutron-energy resolution of time-of-flight (TOF) facilities is nearing the limits of possible. In addition, the use of calorimetric information on the reaction's Q value often allows unambiguous identification of new weak resonances, which are typically masked by strong resonances from isotopes that are inevitable impurities in targets. The presence of previously unobserved resonances then impacts the deduced average resonance spacing even in nuclei that were studied in detail in the past.

Neutron resonance sequences are often considered perfect objects for application and test of predictions by the random matrix theory (RMT) [5]. If the resonance sequences are complete and their positions follow predictions of the Gaussian orthogonal ensemble (GOE) [6], their average spacing can be determined very precisely [5,7], even if the sequences are not very long and consist of a few tens of resonances. However, the completeness of the measured sequences is required for the applicability of these predictions. We show that traditional tests of completeness based on resonance positions are virtually insensitive for measured sequences of such length. Furthermore, the longer sequences are inevitably incomplete due to missing resonances in state-of-art experimental data, at least in rare-earth nuclei. As a result, the uncertainty in the deduced average resonance spacing is dominated by the uncertainty in the number of missing resonances. This can be illustrated on ^{167}Er, one of the nuclei analyzed in this paper. Mulhall performed analysis [8] of the first 113 observed resonances below about 520 eV, and the fraction of missing resonances was determined as 0 and 6% using two different methods [8,9] based on the level positions. These fractions result in inconsistent $D_0 = 4.63(7)$ and 4.35(7) eV, respectively. Moreover, these spacings are inconsistent with $D_0 = 3.80(21)$ eV proposed by Mughabghab [10].

The paper is organized as follows: Sec. II, that gives description of experimental conditions, is followed with the description and application of the multiplicity method to measured nuclei in Sec. III. Section IV then deals with tests of observed sequence completeness and the sensitivity of these tests, and also shows that is very difficult to observe a long complete sequence. Spacing deduced from our analysis is then given in Sec. V, followed with concluding remarks.

II. EXPERIMENT

The neutron capture experiments took place at the moderated spallation neutron source of Lujan Center of LANSCE [11]. A detailed description of the DANCE detector setup and data processing can be found in Refs. [12–16]. Here we restrict ourselves to cover only the basic features and details specific to the Dy and Er capture measurements. Further details specific to Dy measurements can be found in Ref. [17].

A. Experimental setup

At LANSCE 800-MeV protons with a repetition rate of 20 Hz strike a tungsten target producing neutrons with energies ranging from subthermal to several MeV. The Dy or Er samples were located inside the DANCE detector [12,13] at a 20.25 m distance from the neutron source.

The DANCE detector consists of 160 BaF_2 scintillation crystals forming an array with a solid angle of $\simeq 3.5\pi$. The detection efficiency for a 1-MeV photon is 86% and the energy resolutions for 1- and 6-MeV photons are about 16 and 7%, respectively. To reduce the number of neutrons scattered from the sample, a 6-cm-thick ^{6}LiH shell is placed between the sample and the crystals.

The DANCE acquisition system is based on the digitization of signals from all 160 BaF_2 crystals. The Dy measurements were performed with four-channel eight-bit Acquiris DC265 digitizers with a sampling rate of 500 megasamples per second [15]. The more recent Er measurement used 14-bit CAEN V1730 digitizers [16] with 16 individual channels per board and the same sampling rate. The scintillation signal from each BaF_2 crystal is formed by fast (decay time ≈ 600 ps) and slow (decay time ≈ 600 ns) components, which are collected independently. The ratio of these components is used to discriminate against the α background from the natural radioactivity of Ra in the BaF_2 crystals. A precise time stamp of γ-ray arrival is stored and used to construct an event within a certain coincidence window.

The energy calibration of the individual crystals was carried out with a combination of γ-ray sources (^{137}Cs, ^{88}Y, and ^{22}Na) and the intrinsic α radioactivity in the BaF_2 crystals due to ^{226}Ra impurities and its daughters. The latter calibration was performed off-line on a run-by-run basis and allowed to correct for changes in the gain of all crystals throughout the experiment.

All the samples in the form of self-supporting metal foils were prepared at the Oak Ridge National Laboratory. Their masses and isotopic compositions are specified in Table I. We have also seen very small traces (on the level of 0.01%) of Sm and Er in Dy samples. Two experiments were performed for ^{167}Er. The same material was used in these measurements but the mass differed by a factor of 4. The experiment with higher mass allowed us to get sufficient statistics up to a few hundred eV. On the other hand, a very high count rate in the strong low-lying resonances caused changes in the multiplicity distribution obtained with the new CAEN digitizers. The smaller mass sample data then allowed us to check also the strongest low-energy resonances.

B. Data processing

The energies of neutrons impinging on the sample were determined using the time-of-flight technique. The time alignment of the response of individual crystals can be done with a precision of a few ns. All signals are considered to belong to

TABLE I. Mass and isotopic composition of the measured Dy and Er samples. Additional smaller-mass Er measurement was performed with a mass reduced by a factor of 4 to check the behavior of the strong resonances. Also listed are the neutron separation energy S_n of the product nucleus, the range of sum energies E_Σ-gate used in the data processing and the critical energy $E_{\rm crit}$ used in simulations.

Sample	Mass (mg)	Isotope abundance (%)						s_n (MeV)	E_Σ-gate (MeV)	$E_{\rm crit}$ (MeV)
		^{160}Dy	^{161}Dy	^{162}Dy	^{163}Dy	^{164}Dy				
^{161}Dy	31	0.33(2)	95.69(37)	2.52(13)	0.90(8)	0.56(5)		8.197	7.6–8.4	1.87
^{163}Dy	32	0.03(1)	0.36(1)	1.23(2)	96.86(4)	1.52(2)		7.658	7.0–7.8	1.70
		^{162}Er	^{164}Er	^{166}Er	^{167}Er	^{168}Er	^{170}Er			
^{167}Er	20.1	0.02(3)	0.06(6)	2.94(11)	91.52(25)	5.15(11)	0.33(6)	7.771	7.0–8.0	2.20

the same event if they arrive within 6–10 ns, depending on the experiment.

An emitted γ ray does not necessarily deposit all of its energy in a single crystal, but rather in several and often neighboring BaF_2 crystals. Therefore, the number of crystals that are hit during a γ-ray cascade detection is higher than the true multiplicity [14]. To take this into account, we combine all contiguous crystals that fire during an event into clusters. The number of clusters contributing to an event is called the *cluster multiplicity m*.

From individual events, we can construct spectra of sums of deposited γ-ray energies, hereafter called *sum-energy spectra*, for a given neutron energy and multiplicity m. Figure 1 shows such a spectrum, summed for $m = 2$–6, versus the TOF transformed to neutron energy scale for ^{167}Er. We can identify resonances coming from different isotopes via deposited energy profiles. Events with deposited sum energy $E_\Sigma \gtrsim 8$ MeV mainly originate from the neutrons scattered on the sample and subsequently captured on Ba isotopes with $S_n > 8.5$ MeV present in the BaF_2 crystals. Moreover, in the strong resonances, there are events corresponding to the detection of γ rays from more than one capture event within the coincidence window, which are observed up to $E_\Sigma = 2S_n$. Although these events are visible in Fig. 1, their number is very small compared to events with $E_\Sigma \lesssim S_n$. There is also a contribution from the background for $E_\Sigma < 3$ MeV caused by natural β radioactivity in the BaF_2 crystals. In reality, this contribution is restricted dominantly to $m = 1$.

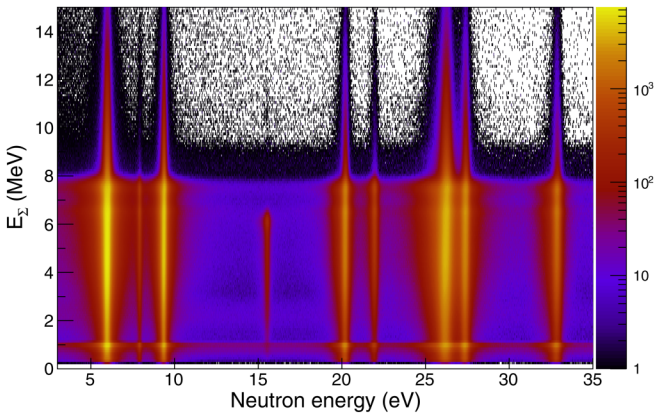

FIG. 1. Sum-energy spectrum vs neutron energy for ^{167}Er higher mass sample. Events with $m = 2$–6 were considered. The resonance just above 15 eV with clearly lower maximal E_Σ is a contaminant from the sample impurity ^{166}Er with $S_n = 6.436$ MeV.

Each sum-energy spectrum in Dy isotopes consists of (i) a peak near the neutron separation energy S_n, which corresponds to the detection of all γ-ray energy emitted in a cascade, and (ii) a low-energy tail, which is formed by events where a part of the emitted γ-ray energy escapes the detection; see Ref. [17]. Erbium sum-energy spectrum is more complicated due to a presence of an isomeric state at an excitation energy of 1.094 MeV with a half-life of about 109 ns. As the lifetime is much larger than the coincidence window, we also see peaks corresponding to cascades ending at the isomeric state and the decay of the isomer.

Sum-energy spectra corresponding to four different Er resonances, normalized to the same number of events with $E_\Sigma =$ 7.0–8.0 MeV and $m \geqslant 2$ are shown in Fig. 2. The sum-energy spectra have different multiplicity distributions for resonances with different spins, which is the key feature used in the spin assignment method described below. Only events in the E_Σ range around the respective S_n were considered in the analysis as indicated in Table I. As mentioned above, the use of these ranges allows for very effective elimination of parasitic resonances from sample impurities.

III. RESONANCE SPIN ASSIGNMENT

A. Spin assignment methods

For the target nucleus with nonzero spin I, the spin J of s-wave neutron resonances can take on two values $J = I \pm 1/2$. Their spins can be determined by several methods that can be divided into three main groups: (i) analysis of transmission, scattering, or capture cross-section measurements [10,18–20], (ii) measurement of transmission using polarized neutrons and samples [21,22], and (iii) detection of differences in γ-ray spectra from decay of resonances with different spins. Several different observables can be checked in the latter case. In the pioneering work, Coceva *et al.* [23] used the ratio of singles to coincidence counts from two scintillation detectors. However, many other quantities can be considered including intensities of γ rays from low-lying levels measured with semiconductor detectors [24,25], the singles/singles, and coincidences/coincidences ratios for different pulse-height regions acquired with C_6D_6 detectors [26], or cascade characteristics measured with 4π segmented detector arrays, e.g., DANCE [4,27,28] or TAC at n_TOF [29].

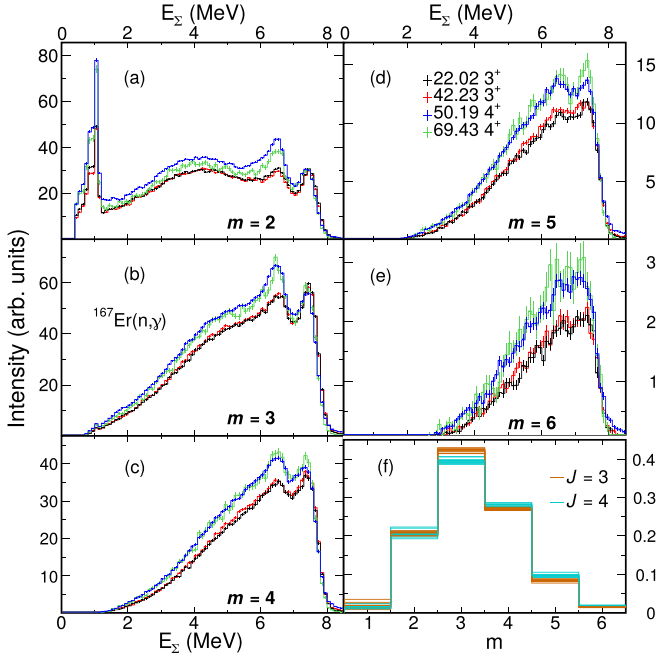

FIG. 2. [(a)–(e)] Sum-energy spectra for individual cluster multiplicities m for four resonances in ^{167}Er. Energies and spins of individual resonances are indicated in the legend. There is a visible distinction between sum-energy spectra of different spins. (f) E_Σ-gated multiplicity distribution deduced from 22 well-isolated resonances (11 of each spins) in ^{167}Er. All spectra are normalized as described in Sec. II B.

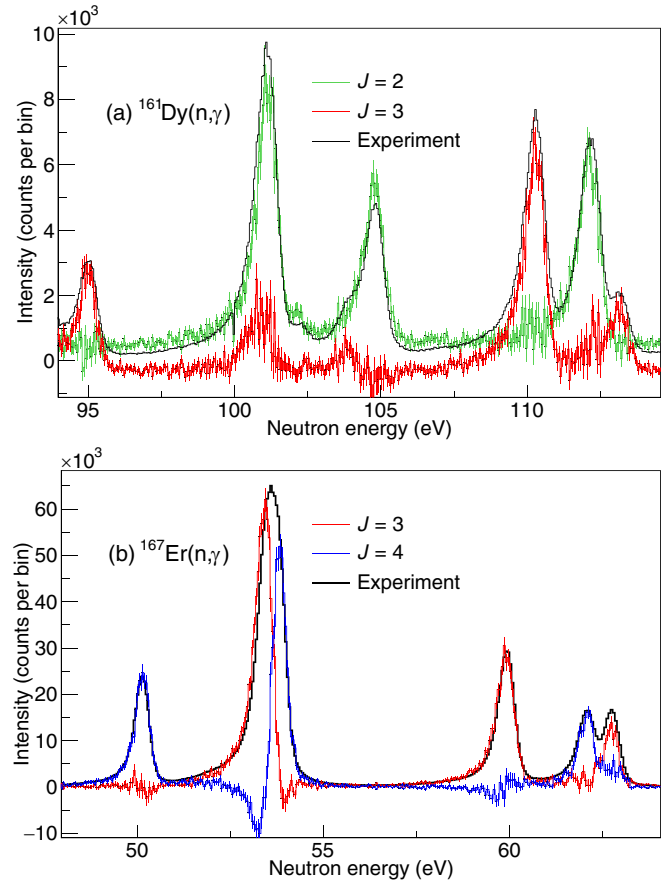

FIG. 3. Experimental and decomposed TOF spectra for ^{161}Dy (a) and ^{167}Er (b). The decompositions were performed using $m =$ 2–6 with two prototypes in both cases. The decompositions show the presence of previously unreported doublets near 101 and 53.5 eV in ^{161}Dy and ^{167}Er, respectively. In the latter case, a clear indication of a doublet presence comes already from the shape of the resonance structure observed in our spectrum. The decomposed shapes nicely agree with the shapes of the neighbor resonances.

B. Optimized γ-multiplicity-based spin assignment method

The γ-multiplicity-based spin assignment method by Bečvář *et al.* [4] is applicable if resonances with different spins display different measured multiplicity distributions. In favorable conditions, it can distinguish very close doublets at low neutron energies, which might remain undetected by other methods, especially those of group (i). The favorable conditions—especially different multiplicity distribution and low, almost TOF-independent background—should be fulfilled in nuclei with high level density and dominant capture cross section, surely rare-earth ones. The measured TOF spectrum is decomposed into contributions belonging to each resonance spin, the method was originally proposed to be used with two different prototypical multiplicity distributions corresponding to two possible spins of s-wave resonances.

In this paper, we adopted a generalized version of the method that allows decomposition of the measured TOF spectrum into several prefixed prototypical multiplicity distributions—we used either two or three prototypes corresponding to two possible spins of s-wave resonances and the background contribution. Several different ranges of multiplicity were tested. The use of only two prototypes—that were taken from well-isolated resonances of different spins—is usually sufficient if only $m \geqslant 2$ spectra are considered. A contribution of the background is mostly visible for $m = 1$ which then requires us to use also the third prototype. This prototype was taken either from the off-resonance region or from an ancillary measurement with a ^{208}Pb sample, which serves as a neutron scatterer, and detected events are hence dominated by the subsequent neutron capture on Ba. The multiplicity distribution of off-resonance events is largely independent of the neutron energy of our interest. The obtained spin decomposition is consistent for all tested choices of m ranges, the number of prototypes, and the selection of the prototype resonances. The obtained spin decomposition is illustrated in Fig. 3 for ^{161}Dy and ^{167}Er.

Intensities of primary transitions fluctuate even among different resonances with the same spin, the expected distribution is a χ^2 with one degree of freedom, known as the Porter-Thomas distribution [30]. As a result, the multiplicity distributions from different resonances of the same spin are not the same. The method for decomposition works only if the differences between resonances with the same spin are smaller than the differences between resonances with different spins. Figure 4 shows the normalized mean multiplicity distributions for 25 and 22 ^{161}Dy resonances with $J = 2$ and 3, respectively. A normalized multiplicity distribution of 22 ^{167}Er resonances (11 of each spins) is also shown in Fig. 2(f). The observed

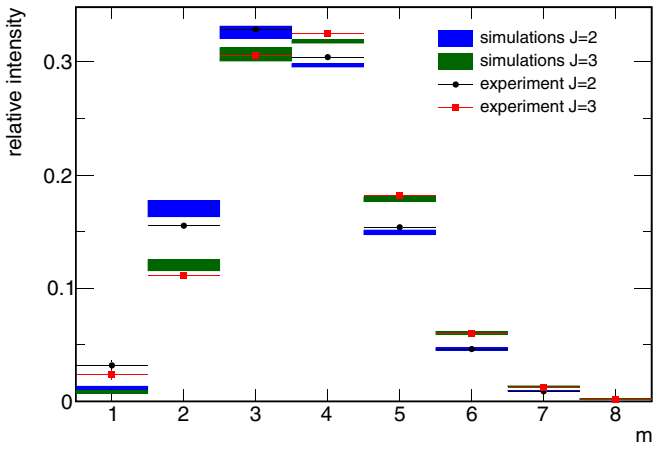

FIG. 4. Comparison of average experimental and simulated multiplicity distribution of ^{161}Dy resonances. Only events with sum energy between 7.6 and 8.4 MeV are used to construct the individual resonance spectra, which are then normalized to their integral for $m \geqslant 2$. The mean and standard deviation of the distributions are calculated using the maximum likelihood fit as described in Ref. [17]. The larger spread of simulated values is due to the random nature of NSRs.

differences indicate that the method should yield unambiguous spin assignment in these nuclei.

The fluctuations in multiplicity distributions from individual resonances lead to imperfections in the decomposition. Naturally, a deviation of decomposed contribution for the correct spin from the total counts is observed. This is accompanied by the appearance of the so-called *ghost resonances* in the other decomposed contributions. The ghost resonances can be either positive or negative and their shape should follow the shape of the actual resonance [4]. For strong and well-isolated resonances of ^{167}Er and ^{161}Dy, we calculated the relative sizes of these ghosts, R, as the ratio of the area of the ghost resonance to the total area of the actual resonance. The average of R depends on the selection of the prototype and is close to zero if the prototypical distributions are close to the average distribution for a given spin. The standard deviation of R was then for decompositions using $m = 2$–6 found to be about 0.12 and 0.09 for both spins in ^{167}Er and ^{161}Dy, respectively. This behavior indicates that the method should uniquely determine the spin in all resonances with sufficient statistics in these nuclei. On the other hand, in ^{163}Dy we observe a couple of resonances with similar decomposed contributions for both J, and the standard deviation of R was found to be at least 0.15 (depending on the prototype resonances). This indicates problems with unambiguous spin assignment in this nucleus.

C. Verification of the method applicability from simulations

The different behavior of decomposed contributions and size of ghost resonances R among different nuclei could be a physical effect related to decay or it could indicate a problem with experimental data for one or more isotopes. To disentangle the origin of the effect, we decided to check the behavior of R from simulations. Specifically, we simulated the γ decay utilizing the Monte Carlo DICEBOX algorithm [31,32]. In these simulations, all information on the level scheme below a certain critical energy $E_{\rm crit}$, listed in Table I, were taken from the ENSDF database [33–35]. Above $E_{\rm crit}$, the statistical model is applied using *a priori* chosen models of NLD and photon strength functions (PSFs). The NLD and PSFs used in simulations were those well reproducing the sum energy and multistep cascade spectra. The analysis of these spectra from ^{161,163}Dy(n, γ) reactions was published in Ref. [17]. Results of an analogous analysis for ^{167}Er(n, γ) will be published soon. In reality, very similar models allow a good description of the spectra also for previously analyzed even-even Gd isotopes [36,37].

The fluctuations in the positions of simulated levels and the Porter-Thomas fluctuations of transition intensities, present in the DICEBOX algorithm, can produce an enormous number of different simulated nuclei. Let us denote one simulated set of all levels below the capturing state and their properties (energy, spin, parity, branching intensities) as a *nuclear suprarealization* (NSR). In order to reproduce the behavior of various resonances with the same spin and parity that differ only in intensities of the primary transitions, we randomly generated primary transition intensities within any given NSR several times. Each set of primary decay branching intensities within a given NSR is referred to as a *nuclear realization* (NR).

The detector response to generated γ cascades was applied via simulations with the Monte Carlo GEANT4 [38] based code [14]. Simulated sum-energy spectra were calculated for each NR. The simulated multiplicity distributions, averaged over 50 NSR and 50 NR within each NSR, are shown in Fig. 4. The larger spread of simulated values with respect to the experiment is due to the random nature of NSRs.

Similarly to the experiment, we checked the distribution of R from simulations. We found that the distribution within each NSR was close to a normal one with a mean again depending on the selection of the prototype and standard deviations of about 0.12(2), 0.09(2), and 0.25(6) for ^{167}Er, ^{161}Dy, and ^{163}Dy, respectively; the uncertainty in R corresponds to spread between NSRs and the mean values slightly (within the listed uncertainty) depend on the resonance spin. The results from simulations perfectly agree with the aforementioned experimental values of R for ^{161}Dy and ^{167}Er, and allow for resonances with similar decomposed contributions for both spins in ^{163}Dy. This behavior means that the applicability of the used γ-multiplicity-based spin assignment method needs to be checked individually for each nucleus. Such a check requires knowledge of a realistic description of γ-ray decay. Fortunately, this knowledge is available for all three tested nuclei from analyses of multistep cascade spectra. However, an unambiguous spin assignment can be made even for the vast majority or ^{163}Dy resonances.

D. Results

The spectra were analyzed up to neutron energies specified for each isotope in the following subsections. In the lower energy part of the interval, the spin was (at least tentatively) assigned to all observed resonances. The lowering statistics

and worsening energy resolution of the facility with increasing neutron energy make unambiguous disentanglement of complex resonance structures and the spin assignment more difficult. As a result, above certain neutron energy—determined for each isotope individually—only resonances with the firm or tentative spin assignment made from our data are listed.

The resonance spins from our method are overall in very good agreement with available ones; more differences are seen only for ^{161}Dy with respect to the Rensselaer Polytechnic Institute (RPI) data [39].

In all three isotopes, our method allowed clear identification of previously unreported doublets of complementary spins; see Tables VIII–X. and examples in Fig. 3. A doublet was introduced only if the energy difference between individual components was statistically significant and the observed structure thus cannot be the ghost resonance.

In addition to previously reported resonances, we also observed several new (weak) isolated ones in both Dy isotopes. Their observation was allowed by the availability of the sum-energy spectra, i.e., calorimetric information, as these resonances are at very similar neutron energies to resonances in other Dy isotopes. Correct assignment to a particular isotope was then confirmed by cross checking spectra for both odd-*A* Dy isotopes, which are major contaminants in the samples. A few comments on specific resonances in individual nuclei can be found in the following subsections.

We note that we did not try to determine resonance energies using dedicated software for resonance shape fitting (SAMMY, REFIT). Nevertheless, our rough estimates based on the observed positions of maxima do not show any deviation from literature values.

1. ^{161}Dy

We analyzed spectra up to neutron energy of 400 eV; above 209 eV, only resonances with firmly or tentatively assigned spin are reported. Our results are listed in Table VIII together with the values from Mughabghab's atlas [10] and the recent RPI work [39]. Resonance parameters (without spins) below 300 eV are also available in a recent paper by Shin *et al.* [40] from the Accurate Neutron-Nucleus Reaction Measurement Instrument (ANNRI) facility at Japan Proton Accelerator Research Complex (J-PARC). Several singlet resonances from Ref. [10] were reported as doublets in Refs. [39,40]. For some of these, we confirm the doublet character, e.g., the structure around 77 eV. Moreover, we observe several additional complex structures, and the doublet near 101 eV is shown in Fig. 3(a).

On the other hand, we do not observe all the resonances reported in the RPI work [39]. Specifically, a doublet structure near 138 eV was proposed with a neutron width ratio of about 1:4 and an energy difference of about 0.5 eV. We do not see any hint of a doublet structure here, in agreement with Refs. [40,41]. Further, the sum-energy spectrum of a resonance reported at 155.1 eV is inconsistent with other ^{161}Dy resonances. Both resonance energy and sum-energy spectrum are compatible with a resonance in ^{163}Dy. Finally, we cannot confirm the presence of the $J = 3$ resonance at 165.9 eV, again in agreement with Refs. [40,41]. If it existed, it would be on the tail of a much stronger $J = 3$ resonance at 166.6 eV.

The reported Γ_n^0 of the 338 eV resonance [10] is about 15× higher than the expected value. Such a high value has a probability of only about 10^{-4} to occur. In addition, the RPI measurement reported very high $\Gamma_\gamma = 172$ meV for this resonance, which is inconsistent with predictions of the statistical model allowing only a few percent fluctuation of this quantity [17]. Our data clearly indicate a presence of a doublet at this energy.

2. ^{163}Dy

Our results are reported in Table IX, the maximum neutron energy is 485 eV, and only a few resonances with a firm spin assignment are reported above 402 eV. We again compare resonance spins to Mughabghab's atlas [10] and the RPI work [39]. The resonance energies and widths up to 300 eV were also determined by Shin *et al.* [40].

Results of Sec. III C indicated larger fluctuations in the multiplicity distribution that could manifest themselves as a presence of significant ghost resonances, whose allowed size can even prevent spin determination. Indeed, we see a few resonances where deduced contributions of both spins differ by less than a factor of 2. They appear near 55.9, 72.0, 120.3, 145.0, and 288 eV. For the last three cases, the energy shift between the two decomposed contributions is insignificant. Moreover, the stronger contributions are consistent with the resonance spins from literature. Hence, we claim that our data is consistent with a singlet resonance in these cases. A doublet with energy difference 0.3 eV was reported in [10] near 72 eV. In reality, we do not see any sign of a doublet in our data (in accord with Refs. [39,40]). The energy shift between the decomposed contributions is insignificant, indicating only a presence of a strong ghost resonance with $R \approx 0.4$ near 72.0 eV. Finally, a single resonance was reported in the literature at 55.9 eV. However, our decomposition indicates two resonances with an energy difference of about 0.03 eV and similar strength. Although the energy difference is small, it is incompatible with a presence of a ghost resonance. Moreover, large radiative width of this resonance reported in Refs. [39,40] already indicates a possible multiplet structure at this energy. We report a doublet in Table IX. Nevertheless, in the statistical analysis, we also tested the possibility of $J = 3$ singlet.

A doublet near 298 eV was reported in Ref. [39] with an energy separation of about 0.8 eV and $J = 2$ of both resonances. The same proposed spin of both resonances makes an observation of the possible doublet difficult. Nevertheless, we should still be able to identify a doublet presence from the observed resonance shape. However, we do not see any sign of it in accord with Refs. [40,41]. If a lower energy resonance was present, it would need to be much weaker than the one reported from the RPI measurement (and be of $J = 2$).

3. ^{167}Er

All resonance structures were analyzed up to energy 285 eV, and firm and tentative spin assignments are presented up to 670 eV; see Table X. Our results are compared to Mughabghab's atlas [10]. Most notably we clearly identified six doublets below 285 eV, which were all reported as singlet

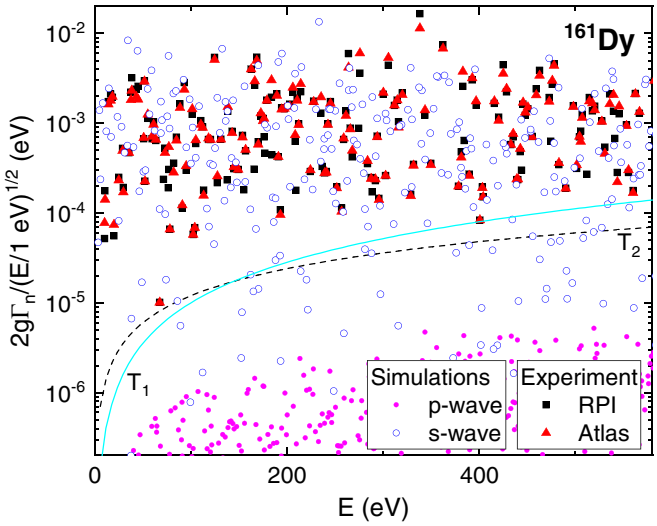

FIG. 5. Experimental data from Mughabghab's atlas [10] and RPI work [39] on $2g\Gamma_n/\sqrt{E/1\text{eV}}$ as a function of neutron energy E for ^{161}Dy. Shown are also thresholds T_1 and T_2 used in the analysis of subthreshold resonances and one random simulated sequence of resonances obtained using $D_0 = 2.15$ eV, $S_0 = 2.0 \times 10^{-4}$, $D_1 = 1.16$ eV, and $S_1 = 1.3 \times 10^{-4}$.

resonances therein. In fact, also the first observed resonance structure above 285 eV, reported as a singlet in Ref. [10] at 288.8 eV, is very likely formed by more resonances.

Although we see an indication of a weak resonance at 204 eV (preferably with $J = 4$), its presence cannot be confirmed with a high significance from our data. We thus considered all possibilities (its absence as well both allowed spins) in the statistical analysis below. Nonetheless, as a resonance at the same energy was previously reported [10], its existence is highly probable.

The resonance at 26.34 eV has a large reported Γ_n^0, about 12 times larger than the expectation value [10]. Similar to the 338 eV resonance in ^{161}Dy, such a high value has a low probability to occur. No indication of a multiplet structure is found in our data in this case.

IV. RESONANCE SEQUENCES COMPLETENESS

As mentioned in the introduction, the average spacing D_0 can be determined with a very low uncertainty [5,7] if the resonance sequences are complete and their positions follow RMT predictions of GOE [6]. The information on the completeness or the exact number of missing resonances is thus essential for precise D_0 (or equivalently NLD) determination.

The measured sequences are, unfortunately, often either incomplete due to missing resonances or contaminated with p-wave ones. To assess the latter, we checked the allowed strength—in terms of neutron width—of p-wave resonances in tested nuclei using S_1 from Ref. [10]. A chance that any observed resonance is of p-wave origin was found to be extremely small below neutron energy of about one keV, and the expected situation is illustrated for ^{161}Dy in Fig. 5.

There are two different ways an s-wave resonance can be missed: (i) It is a part of a close doublet or (ii) it is a singlet too weak to be observed, hereafter denoted as a subthreshold resonance. In even-even targets, the first option does not usually play any significant role as resonances of the same spin should not be very close to each other due to expected repulsion in energies [6]. However, the presence of two possible spins for non-zero-spin targets makes this reason relevant. The second option is common for all targets and arises from expected Porter-Thomas fluctuations [30] of individual Γ_n^0.

TABLE II. Fraction of complete mixed-spin sequences F_0^m and the mode of distribution of subthreshold resonances for different $E_{\max}$ and both adopted thresholds. Parameters used in simulations were $S_0 = 2.0 \times 10^{-4}$ and $D_0 = 2.15, 6.4, 3.85$ eV for ^{161}Dy, ^{163}Dy, and ^{167}Er, respectively. For the relation between mixed- and pure-spin sequences, see the text.

Nucleus	Threshold	$F_0^m \times 10^3$/Mode		
	$E_{\max}$ (eV)	86	135	209
^{161}Dy	T_1	179/1	21/3	<0.1/8
	T_2	100/2	10/4	<0.1/8
	$E_{\max}$ (eV)	215	290	402
^{163}Dy	T_1	187/1	54/2	6/5
	T_2	170/1	59/2	10/4
	$E_{\max}$ (eV)	135	200	285
^{167}Er	T_1	280/1	84/2	12/4
	T_2	152/1	37/3	4/5

The option (i) was addressed in Sec. III. In this section, we estimate the number of subthreshold resonances using the fluctuation properties of Γ_n^0 as well as GOE predictions of statistical properties of resonance energies. The procedure of simulating the artificial resonance sequences is described in Appendix A.

For the statistical tests of completeness, we adopted resonance sequences for three different maximum neutron energies $E_{\max}$ in each nucleus. Specifically, we considered resonances up to $E_{\max} = 86$, 135, and 209 eV in ^{161}Dy; 215, 290, and 402 eV in ^{161}Dy; and 135, 200, and 285 eV in ^{167}Er. The highest considered $E_{\max}$ was determined by the ambiguity of the spin decomposition, usually by a presence of a resonance to which we were unable to assign a spin. The lower $E_{\max}$ were then determined by an uncertain assigned spin just above the chosen energy and/or to keep a certain probability for the sequence to be complete; see Table II. For specific cases, see footnotes in Tabs. III–V and Sec. III D; we have tested all reasonable alternatives.

A. Estimates based on neutron width fluctuations

The quantity that determines the observability of a singlet resonance in a neutron capture measurement is its capture kernel. For the weakest resonances in the rare-earth region, it holds that $\Gamma_n \ll \Gamma_\gamma$, $\Gamma_\gamma \approx 0.1$ eV, fluctuating only by a few percent. Hence, their capture kernel can be approximated by $g\Gamma_n$. The analysis is traditionally performed using $2g\Gamma_n/\sqrt{E/1\,\text{eV}}$, which is for s-wave resonances equivalent to the $2g\Gamma_n^0$.

Unfortunately, the exact form of the observability threshold is not known as it depends on specific experimental

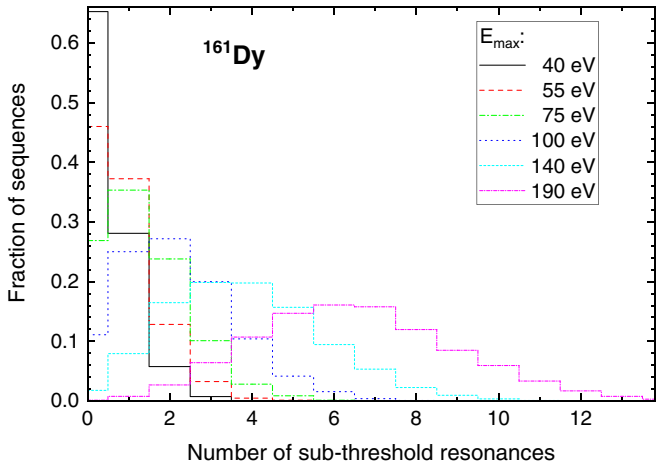

FIG. 6. Distribution of number of subthreshold s-wave resonances for a few maximum neutron energies in ^{161}Dy and T_1 threshold. The simulations used $D_0 = 2.15$ eV and $S_0 = 2.0 \times 10^{-4}$.

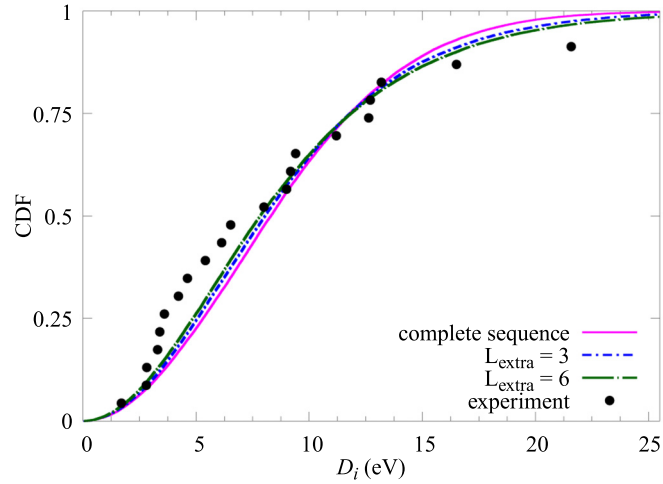

FIG. 7. Cumulative distribution function (CDF) of simulated NNSD for a complete pure-spin $L_{\max} = 23$ sequence together with sequences where $L_{\text{extra}} = 3$ and 6 resonances were missed. The experimental D_i values for the $L_{\max} = 23$ sequence of $J^\pi = 3^+$ resonances in ^{167}Er are shown as black points. As presented in Table V, none of the simulated options is rejected using our criterion introduced in Sec. IV B.

conditions. It is usually assumed that the threshold can be reasonably approximated with a power law in neutron energy. We applied the $E^{3/2}$ and E neutron energy dependence of the threshold, and absolute scaling was adjusted individually using the weakest observed resonances. Specifically, we tested $T_1 = C_1 E^{3/2}$ and $T_2 = C_2 E$ with the constants $C_1 = 1 \times 10^{-8}$ eV$^{-1/2}$ and $C_2 = 1.2 \times 10^{-7}$ for the Dy targets, and $C_1 = 0.6 \times 10^{-8}$ eV$^{-1/2}$ and $C_2 = 1.1 \times 10^{-7}$ for the Er target.

For ^{161}Dy, these thresholds are shown in Fig. 5 together with experimental $2g\Gamma_n^0$ values from Refs. [10,39]—note that the $g\Gamma_n^0$ values therein and in Ref. [40] are very similar, at least for the weakest observed resonances. Available data on $g\Gamma_n^0$ indicate that the threshold in ^{163}Dy is likely similar to and in ^{167}Er slightly lower than in ^{161}Dy—this is reflected by individual C_1 and C_2 values. The strengths of all newly proposed resonances in this work are definitely well above these thresholds.

The simulated sequence in Fig. 5 indicates that completeness of the observed one cannot be guaranteed even for the lowest $E_{\max}$. The distribution of the number of subthreshold resonances in simulated mixed-spin sequences is then shown in Fig. 6 for a few maximum neutron energies for ^{161}Dy. Let us denote the fraction of complete sequences, i.e., sequences with zero number of subthreshold resonances, as F_0. Distributions for other isotopes have similar shapes if F_0 is comparable to the presented one. The same fraction F_0 appears at different maximum neutron energies in studied isotopes due to different D_0 and applied thresholds. Table II then gives F_0^m and the most probable number of subthreshold resonances (mode of the distribution) for the three tested $E_{\max}$ and both thresholds; the superscript m indicates mixed-spin sequences. The dependence of obtained distribution on S_0 and D_0 is relatively weak for fixed $E_{\max}$. In general, the analysis indicates that a half, quarter, and tenth of complete sequences can be expected for maximum neutron energies corresponding to about 25, 30, and 40 resonances; the exact length depends on the nucleus and threshold.

We verified that the fraction F_0 and mode of the distribution for pure spin sequences can be deduced in the following way. Let us denote by F_0^-, F_0^+ the fractions for lower and higher spin sequences, respectively. Then it holds that $F_0^m = F_0^- F_0^+$, which corresponds to the independence of the two factors. At the same time, it holds that $F_0^-/F_0^+ = D_0^-/D_0^+$, where D_0^- and D_0^+ are the average resonance spacings for lower and higher spins, respectively. For a given fraction F_0, the mode can be estimated with help of Fig. 6. The sum of modes of the two pure-spin sequences can differ by unity from the mode for the mixed-spin sequence as a consequence of rounding.

B. Tests of completeness based on resonance positions

If we assume that resonance sequences, both pure in spin and a mixture of two spins, follow the RMT predictions of the GOE, we can test their completeness using several different statistics [5].

The most simple one is the nearest neighbor spacings distribution (NNSD), which is expected to be very close to the Wigner distribution [42]. Example of cumulative distribution of NNSD for ^{167}Er can be found in Fig. 7. In addition, GOE predicts correlation in level positions. These short- and long-range correlations are usually characterized by the correlation coefficient of two adjacent spacings $\rho(D_i, D_{i+1})$, and by the Δ_3 statistic for level positions. The distribution of these quantities was deduced from simulations for complete sequences of the same length $L_{\max}$ as their experimental counterpart. Furthermore, we have generated longer sequences with $L_{\max} + L_{\text{extra}}$ resonances, from which we then randomly removed L_{extra} inner resonances to mimic the experimental case of missing resonances. The statistics were calculated for these sequences in the same manner as for the complete ones. Results for incomplete sequences allow checking the sensitivity

TABLE III. Results of the statistical analysis of ^{161}Dy resonance sequences. The range of L_{extra} for which the sequence is compatible with GOE predictions for Δ_3, NNSD (column labeled D_i) and correlation coefficient ρ is given, e.g., "0+" means $L_{\text{extra}} \geqslant 0$. The compatibility criteria are described in Sec. IV B.

			$J^\pi = 2^+$			$J^\pi = 3^+$			Mixed		
$E_{\max}$(eV)	$L^-_{\max}$	$L^+_{\max}$	Δ_3	D_i	ρ	Δ_3	D_i	ρ	Δ_3	D_i	ρ
86	16	22	1+	1+	0+	2+	1+	0+	0+	0+	0+
135	25	31	0+	1+	0+	0+	1+	0+	0–3	0+	0+
209[a]	37	47	1+	1+	0+	9+	1+	0+	12+	0+	9+

[a]No 165.9 eV; if considered with $J^\pi = 3^+$ results identical.

of different statistics to missing resonances. We checked incomplete sequences only with $L_{\text{extra}} \lesssim L_{\max}/3$, because higher values are highly unlikely as showed in Sec. IV A.

Consistency of the experimental data with the GOE predictions is summarized in Tables III–V for ^{161}Dy, ^{163}Dy, and ^{167}Er, respectively. The values in these tables indicate the range of L_{extra} for which the sequence is compatible with GOE predictions; e.g., the symbol 0+ corresponds to $L_{\text{extra}} \geqslant 0$. The presence of the symbol "0+" in a majority of cases means that predictions with all tested L_{extra} were compatible with experimental data and no estimate of the number of missing resonances can be made.

The allowed number of missing resonances for a given $L_{\max}$ was assessed in the following way: For each value of L_{extra}, we calculated the NNSD distribution from GOE-generated sequences and evaluated the experimental p value using the statistic proposed by Zhang [43].[1] If this p value fell to the 95.45% central interval, corresponding to $\pm 2\sigma$ interval of the normal distribution, the experimental NNSD was considered to be consistent with the simulated counterpart.

The correlation coefficient $\rho(D_i, D_{i+1})$ was calculated for the full length $L_{\max}$ of the sequence in question using all adjacent spacing pairs. The cumulative distributions of $\rho(D_i, D_{i+1})$ was obtained from simulations. The compatibility with the GOE predictions for $L_{\text{extra}} = 0, \ldots, L_{\max}/3$ was again evaluated using the 95.45% central interval.[2] An example is shown in Fig. 8 for pure $L_{\max} = 23$ sequence for several values of L_{extra} together with the experimental value for ^{167}Er sequence of the same length corresponding to the $J^\pi = 3^+$ resonances up to $E_{\max} = 200$ eV.

The Δ_3 statistic was used in the form

$$\Delta_3(L) = \left\langle \min_{a,b} \frac{1}{E_{i+L-1} - E_i} \int_{E_i}^{E_{i+L-1}} dE[\mathcal{N}(E) - aE + b]^2 \right\rangle_i, \tag{1}$$

where E_i is the energy of i^{th} resonance, $\mathcal{N}(E)$ is the cumulative level number function, and a and b are parameters of the linear fit to the function $\mathcal{N}(E)$. For a given L, the minimization is made separately for each allowed value of i, and then the averaging is done over all allowed values of i, which satisfy conditions $1 \leqslant i$ and $(i + L - 1) \leqslant L_{\max}$. The Δ_3 was calculated for $L = 3, \ldots, L_{\max}$ from experimental sequences, and the distribution of Δ_3 for all these values of L was obtained from simulated sequences. Traditionally, completeness of experimental sequences was judged by the compatibility of $\Delta_3^{\text{exp}}(L_{\max})$ with the distribution of simulated or analytically derived $\Delta_3(L_{\max})$ [7,45]. To take into account behavior for all L, we count—for a given experimental resonance sequence—the number of $\Delta_3^{\text{exp}}(L)$ points outside of the 95.45% central interval derived from the simulations; note that the corridor is asymmetric. Then we check the probability that a simulated sequence has that or higher number of $\Delta_3(L)$ points outside of the same corridors. If this probability is 4.55% or lower, we reject the hypothesis that the experimental sequence behaves in accord with the simulated case. In Fig. 9, we illustrate the behavior of experimental and simulated Δ_3 for two cases of mixed-spin sequences.

We determined the consistency of the experimental data with simulations using all three aforementioned statistics for

[1]This statistic was found to be usually more sensitive than the traditionally used Kolmogorov-Smirnov or Anderson-Darling ones.

TABLE IV. Results of the statistical analysis of ^{163}Dy resonance sequences. The meaning of columns is the same as in Table III. The different sequence versions are explained by the respective footnotes; see Sec. III D 2 for details.

			$J^\pi = 2^-$			$J^\pi = 3^-$			Mixed		
$E_{\max}$(eV)	$L^-_{\max}$	$L^+_{\max}$	Δ_3	D_i	ρ	Δ_3	D_i	ρ	Δ_3	D_i	ρ
215[a]	16	18	2+	1+	0+	0+	0+	0+	0+	0+	0+
215[b]	15	18	0+	0+	0+	0+	0+	0+	0+	0+	0+
290[a]	19	24	2+	2+	0+	0+	0+	0+	0+	0+	2+
290[b]	18	24	1+	1+	0+	0+	0+	0+	0+	0+	0+
402[a]	24	34	5+	1+	2+	0+	0+	0+	0+	0+	0+
402[b]	23	34	2+	0+	1+	0+	0+	0+	0+	0+	0+

[a]Doublet considered around 55.85 eV.
[b]Singlet 3^- at 55.85 eV.

TABLE V. Results of the statistical analysis of ^{167}Er resonance sequences. The meaning of columns is the same as in Table III, the symbol × indicates inconsistence with all L_{extra} values. The different sequence versions are explained by the respective footnotes; see Sec. III D 3 for details.

			$J^\pi = 3^+$			$J^\pi = 4^+$			Mixed		
$E_{\max}$(eV)	$L^-_{\max}$	$L^+_{\max}$	Δ_3	D_i	ρ	Δ_3	D_i	ρ	Δ_3	D_i	ρ
135	18	17	0–4	0+	0	0+	0+	0+	0+	0+	0+
200	23	27	0+	0+	×	1+	0+	0+	0+	0+	0+
285[a]	29	39	1+	0+	0+	2+	0+	0+	1+	0+	0+
285[b]	30	39	0+	0+	0+	2+	0+	0+	0+	0+	0+
285[b]	29	40	1+	0+	0+	2+	0+	0+	0+	0+	0+

[a]No 204 eV.
[b]204 eV 3^+.
[c]204 eV 4^+.

[2]Experimental $\rho(D_i, D_{i+1})$ for individual checked sequences and the corresponding p value can be found in the Supplemental Material [44].

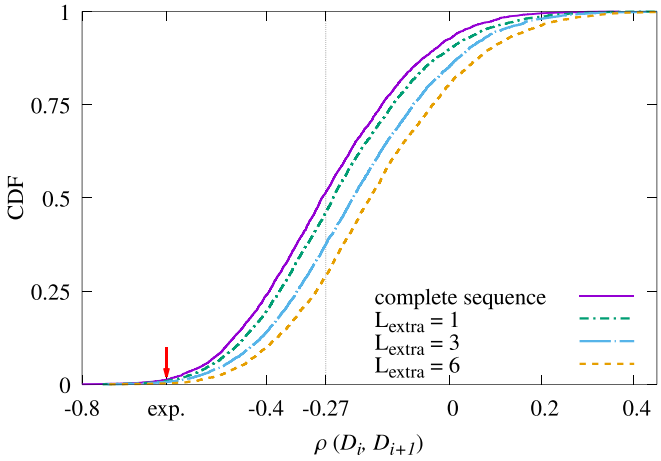

FIG. 8. CDF of the simulated correlation coefficient $\rho(D_i, D_{i+1})$ for a complete pure-spin $L_{max} = 23$ sequence together with sequences where $L_{extra} = 1$, 3, and 6 resonances were missed. The experimental correlation coefficient of -0.6164 for the $L_{max} = 23$ sequence of $J^\pi = 3^+$ resonances in ^{167}Er is shown as a red mark. The corresponding CDF value is 0.0127 for the complete sequence and lower for any sequence with $L_{extra} \geqslant 1$. The RMT using GOE predicts mean value of -0.27 [7], which is displayed as a dashed line.

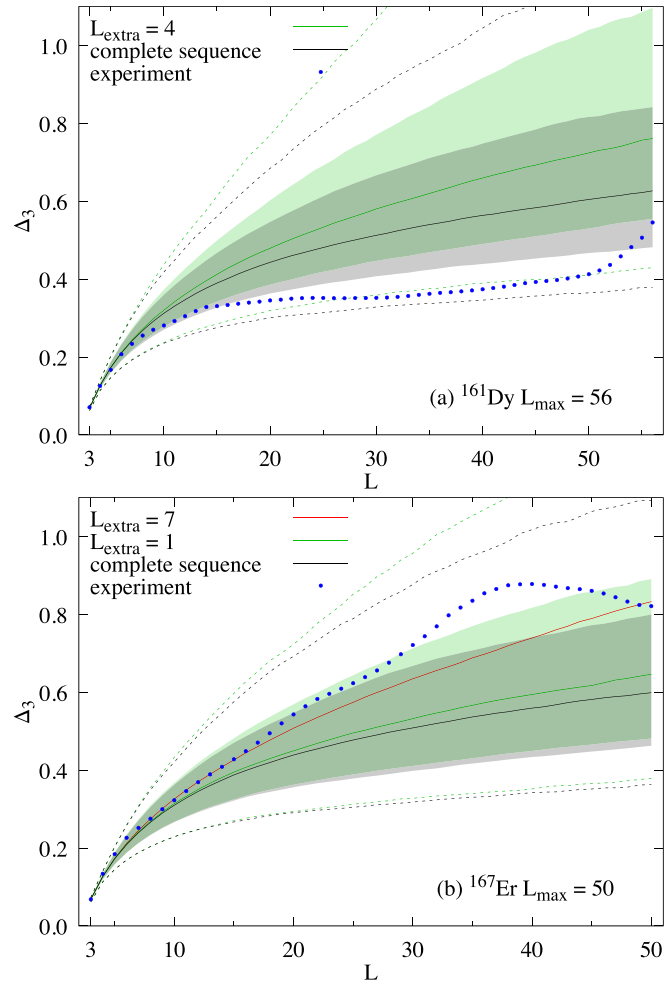

FIG. 9. The Δ_3 statistic as a function of L calculated for experimental mixed-spin sequences of ^{161}Dy (a) and ^{167}Er (b) are compared to their simulated counterparts; the full lines depict the mean values, the corridors correspond to 68.27% central interval, and the dashed lines show the edges of 95.45% central interval.

three different maximum energies. As evident from allowed ranges in Tables III–V, the sensitivity of all three statistics, further discussed in Appendix B, is very restricted—usually a very broad range of L_{extra} is allowed. In some cases ($L_{extra} = 1+, 2+, ...$) we were able to reject the possibility of a complete sequence or even a sequence with a small number of missing resonances. Only in a few cases we were able to give the maximum number of allowed missing resonances. In Fig. 9, the ^{161}Dy sequence with $E_{max} = 135$ eV is compared to GOE predictions for complete sequence and for sequence with $L_{extra} = 4$; the compatibility of experiment with the latter is rejected based on our criterion. The ^{167}Er sequence with $E_{max} = 200$ eV is compatible with all tested values of $L_{extra} = 0, ..., 17$ using our criterion; its value of $\Delta_3(L_{max})$ is best matched by simulations with $L_{extra} = 7$.

Overall, the Δ_3 seems to be the most restrictive. However, also other statistics have some predictive power in specific cases. Despite the restricted sensitivity of the statistics (see details in Appendix B), several checked sequences are evaluated as incomplete, consistent with findings based on Porter-Thomas fluctuations of reduced neutron widths presented in Sec. IV A. There are no contradictory cases.

In connection with the facts presented above and in Appendix B, we would like to elaborate on the example mentioned in the introduction—completeness of sequence of the first 113 resonances below 520 eV checked by Mulhall [8].[3]

The analysis using the Δ_3 statistic indicated 6% of missing resonances while the approach from Ref. [9] a complete sequence. Our criterion using Δ_3 allows three and more missing resonances for this mixed-spin sequence. We would like to note that the number of subthreshold resonances estimated with the T_1 threshold below 520 eV forms a distribution close to the normal one with a mean of ≈12.5 and standard deviation ≈3.5. In addition to Ref. [10], we identified six new above-threshold resonances below 285 eV; see Table X. We can expect a few additional unreported above-threshold resonances between 285 and 520 eV. The expectation number of missing resonances in the sequence from Ref. [10] deduced from the Δ_3 statistic and $g\Gamma_n$ fluctuations is thus consistent and significantly higher than indicated by Mulhall [8]. We note that to reproduce D_0 from our analysis below $E_{max} = 285$ eV (see Sec. V), about 20 missed resonances (corresponding to ≈18%) need to be added to the sequence below 520 eV from Mughabghab's atlas [10].

[3]Resonances from ENDF/Mughabghab available at that time were adopted by Mulhall [8]. The resonances energies in the present ENDF/Mughabghab [10] are slightly different but do not have any impact on results.

TABLE VI. Deduced average resonance spacing D_0 for pure and mixed-spin sequences; D_0^- and D_0^+ stand for spacing corresponding to lower and higher resonance spin, respectively. For details on D_0 determination, see Sec. V.

	E_{max}(eV)	D_0^-(eV)	D_0^+(eV)	D_0(eV)
^{161}Dy	86	4.56(28)	3.53(18)	2.04(8)
	135	4.74(29)	4.03(21)	2.25(7)
	209	5.14(24)	3.61(9)	2.15(5)
^{163}Dy[a]	215	11.69(73)	11.06(82)	5.95(28)
	290	14.07(83)	10.82(68)	6.34(28)
	402	13.70(60)	10.75(57)	6.39(24)
^{167}Er	135	7.46(51)	7.87(58)	3.72(19)
	200	8.49(50)	6.87(34)	3.79(15)
	285[b]	9.03(48)	6.70(25)	3.86(12)

[a]Doublet considered around 55.85 eV.
[b]204 eV 4^+.

V. AVERAGE RESONANCE SPACING

If the observed sequence is complete and free of any contamination, the optimum statistic proposed by Dyson and Mehta [5] allows spacing determination with the relative uncertainty of $4/(\sqrt{2}\pi)/N \sim 0.9/N$ for pure and $4/\pi/N \sim 1.27/N$ for mixed-spin sequences of two spins if the level positions follow the predictions of GOE. In practice, the uncertainties based on experimental data must be larger due to uncertainty related to the sequence completeness. Some corrections to unobserved resonances were applied to estimate the average resonance spacing in the past, e.g., in compilations [10,46] and for Dy isotopes by Liou *et al.* [41]. Unfortunately, these corrections are not well documented.

We determined average resonance spacing for both pure-spin (D_0^-, D_0^+ for lower and higher spins, respectively) and mixed-spin (D_0) sequences assuming that the probability distribution of the number of subthreshold resonances due to Porter-Thomas fluctuations is known. This distribution was obtained from simulations; see, e.g., Fig. 6.

The spacing was obtained from the energy difference between the first and last observed resonance. We assumed that the actual position of the last resonance can fluctuate according to GOE predictions [5] and considered only the numbers of missing resonances allowed by the Δ_3 statistic as specified in Tables III–V. For mixed-spin sequences, we considered the stronger of the Δ_3 restrictions from pure- or mixed-spin ones. Spacing obtained with T_1 threshold is listed in Table VI; values with T_2 threshold differ at maximum by about a third of the listed uncertainty. Although uncertain spin assignment might impact D_0^- and D_0^+, it has no impact on D_0. Spins indicated in DANCE column of Tables VIII–X were used for pure-spin sequences. Spacings deduced from different E_{max} are compatible.

We also checked a possibility for spacing determination from even higher E_{max}. We found that the broadening of the distribution of subthreshold resonances with E_{max} (see Fig. 6) prevents a significant reduction of the spacing uncertainty. In addition, as indicated from our analysis in Sec. III, it is difficult to identify all above-threshold resonances even at low neutron energies; even more of these resonances can be expected with increasing E_{max}. Spacing determination from higher E_{max} thus definitely requires the use of a higher threshold, which leads to an additional broadening of the distribution of subthreshold resonances and prevents reaching

TABLE VII. Comparison of D_0 deduced in this work with literature values. Our data (DANCE) correspond to the highest E_{max} given in Table VI. For details on individual literature values, see Sec. V.

	D_0 (eV)		
Source	^{161}Dy	^{163}Dy	^{167}Er
DANCE	2.15(5)	6.39(24)	3.86(12)
Liou *et al.* [7,41]	2.67(13)	6.85(54)	4.06(17)
Shin *et al.* [39]	2.59(1)	6.90(8)	
Shin *et al.* [40]	2.31(23)	6.91(59)	
Mughabghab [10]	2.08(15)	6.99(30)	3.80(21)
RIPL-3 [46]	2.40(20)	6.80(60)	4.20(30)

TABLE VIII. Resonances in ^{161}Dy(n,γ): The energies and spins are from Mughabghab's compilation (Atlas) [10], RPI work [39] and present analysis (DANCE). Above 209 eV only resonances with firmly or tentatively assigned spin are reported. For details see Sec. III D 1. Electronic version of the table is available in Suppl. Mat. [44].

E_{res} (eV)			J_{res}		
Atlas	RPI	DANCE[a]	Atlas	RPI	DANCE
2.71	–		3	–	3
3.68	–		2	–	2
4.33	–		2	–	2
7.74	–		3	–	3
10.26	10.3		2	2	2
10.85	10.9		3	3	3
12.65	–		3	–	3
14.31	14.3		2	2	2
16.67	16.7		3	3	3
18.48	18.5		2	2	2
–	–	19.8	–	–	(3)
20.24	20.2		(3)	2	3
25.22	25.2		2	2	2
29.04	29.1		2	2	2
29.92	29.9	29.89	3	3	2
		29.95			3
35.74	35.7		3	3	3
37.71	37.7		3	3	3
38.51	38.5		3	3	3
43.27	43.3		3	3	3
45.14	45.2		2	2	2
48.8	–		3	–	3
50.86	50.9		3	3	3
51.8	51.7		2	2	2
52.24	52.2		3	3	3
55.19	55.2		2	2	2
59.57	59.6		2	2	2
61.41	61.4		2	2	2
63.64	63.7		3	3	3

TABLE VIII. (*Continued.*)

E_{res} (eV)			J_{res}		
Atlas	RPI	DANCE[a]	Atlas	RPI	DANCE
–	–	64.6	–	–	(3)
67.55	67.6		3	2	(3)
–	71.5		–	2	3
73.17	73.2		3	2	3
[b]77.07	76.7		3	2	2
	77.2			3	3
78.09	78.1		2	3	2
82.27	82.3		2	2	2
85.07	85.1		3	3	3
–	–	86.7	–	–	(2)
88.77	88.8		3	3	3
91.12	91.1		3	2	2
93.29	93.3		3	3	3
95.23	95.2		3	3	3
[b]101.35	101.4	101.15	2	2	3
		101.45			2
102.42	102.4		2	2	2
104.12	104.2		3	3	3
104.98	105.1		2	2	2
110.50	110.5		3	3	3
112.43	112.4		2	2	2
113.44	113.4		3	2	3
118.42	118.5		2	2	2
120.51	120.6		2	2	2
124.65	124.7		2	2	2
127.54	127.6		3	3	3
131.16	131.2		3	3	3
[b]138.38	138.0		3	2	3
	138.5			3	
142.80	142.9		2	2	2
144.83	144.8		3	2	3
–	–	147.5	–	–	3
149.42	149.4		2	3	2
153.80	153.9		2	2	2
–	[b]155.1	–	–	2	–
156.83	156.9		2	2	2
162.59	162.7		3	3	3
–	[b]165.9	–	–	3	–
166.60	166.6		3	2	3
168.61	168.7		2	2	2
170.09	170.2		3	2	3
172.78	172.9	172.72	2	3	2
		172.90			3
175.29	175.3		3	3	3
176.53	176.3		3	3	2
	177.0			2	3
179.05	179.1		3	3	3
183.69	183.8		3	3	3
	184.5			2	2
189.31	189.4	189.26	2	2	2
		189.55			3
191.00	191.1		3	2	3
192.94	193.1		?	2	(3)
194.44	194.5		2	3	2
197.28	197.4		3	2	3

TABLE VIII. (*Continued.*)

E_{res} (eV)			J_{res}		
Atlas	RPI	DANCE[a]	Atlas	RPI	DANCE
202.81	203.0		3	2	3
206.01	206.1		2	2	2
208.50	208.6		2	2	2
210.48	210.6		2	2	2
211.97	212.1		3	3	3
214.15	214.2		2	3	2
224.43	224.4		?	2	3
227.78	227.9	227.67	3	3	3
		227.72			2
235.46	235.5		2	2	2
	236.5			2	3
238.98	239.2		(3)	3	3
240.77	240.9		2	2	2
242.42	242.6		3	3	3
245.25	245.3	245.24	?	3	3
		245.26			2
251.77	251.7		2	2	(2)
256.81	256.8		?	2	3
258.74	258.9		(2)	3	2
261.13	261.3		3	2	3
263.73	263.9		3	2	3
265.62	265.7		(2)	2	2
267.81	268.0		?	3	2
275.66	274.5		3	2	2
	275.8			3	3
283.55	283.7		3	3	3
287.64	287.6		?	3	2
	288.6			3	3
291.89	292.1		2	2	2
293.64	293.9		3	3	3
294.97	295.7		?	2	2
299.92	300.1		(2)	3	2
302.37	302.5		3	3	(3)
305.45	305.5		3	3	3
311.75	311.9		3	3	3
314.78	314.8		?	2	2
315.76	316.1		?	3	3
319.61	319.9		3	2	3
328.68	328.7		(3)	3	(3)
331.31	331.5		?	2	(3)
[b]337.60	338.1	337.31	?	2	3
		339.03			2
343.53	343.6	343.06	?	2	2
		344.42			3
349.53	349.7		?	3	3
361.95	362.2		?	2	3
378.74	378.5		?	3	2
381.24	381.2		?	2	3
383.05	383.0		?	3	2
	384.2			2	(3)
392.41	392.7		?	3	2
396.35	396.5		?	3	2

[a]Resonance energies are rough estimates based on the observed position of maxima.
[b]See discussion in Sec. III D 1.

smaller uncertainty. Nonetheless, tests with higher thresholds and E_{max} yielded D_0 compatible with the presented results.

Deduced D_0 are compared to values available in literature in Table VII. Smaller values compared to Refs. [7,39,40] should not be surprising as no corrections for missing resonances were applied therein. Specifically, Liou *et al.* [7] obtained D_0 assuming a complete observed sequence below 130 eV in ^{167}Er target using optimal statistic [5], and Shin *et al.* [39,40] then determined D_0 in Dy isotopes from a fit to the cumulative distribution of the observed resonances. Very small uncertainty in Ref. [39] originates only from the uncertainty of the fit. Our results are in a very good agreement with Mughabghab [10] for ^{161}Dy and ^{167}Er while almost two standard deviations off for ^{163}Dy. The disagreement for ^{163}Dy can be at least partly attributed to a few newly observed resonances. The agreement in the other two isotopes seems interesting as several new resonances were observed in both ^{161}Dy and ^{167}Er with respect to those listed in Ref. [10], some of them relatively strong. Uncertainties of D_0 in RIPL-3 [46] are larger than in other sources, giving acceptable agreement with our values. Nonetheless, expectation values in RIPL-3 are systematically higher than ours.

Assuming that we correctly assigned all resonance spins we can determine the ratio of spacings for the two s-wave spins (D_0^-/D_0^+). Experimental ratios based on the spacings for pure-spin sequences and maximum E_{max} from Table VI are compared to those of a few NLD models in Fig. 10. Namely, we show predictions based on different spin cut-off parameters proposed in papers of von Egidy and Bucurescu [49,50], and for models available in TALYS 1.8 [47]; for detailed description of individual NLD models, see the manual [48]. We note that some resonance spins are assigned tentatively and the uncertainty of the experimental ratio could thus be larger. In any case, two of the three microscopic models available in TALYS (TAL5[4] and TAL6) predict the ratios that significantly differ from the experiment. The agreement with the rest of the models is significantly better.

For ^{167}Er the ratio $D_0^-/D_0^+ = 0.63(14)$ can be obtained from $D_0^- = 6.8(12)$ eV, $D_0^+ = 10.8(14)$ eV given by Mughabghab [10]. We do not fully understand a significant difference with respect to our values, although a small change can be expected due to observation of a few new 3^+ resonances at low neutron energies.

VI. CONCLUSIONS

The γ rays following radiative neutron capture on ^{161,163}Dy and ^{167}Er samples were measured with the highly segmented γ-ray calorimeter Detector for Advanced Neutron Capture Experiments at the Los Alamos Neutron Science Center. The γ-ray cascade energies for different multiplicities were gathered as a function of neutron energy. Using the generalized

[4]The Hartree-Fock-Bogoliubov plus combinatorial NLD model presented at RIPL-3 website is identical to TAL5 for positive parity, but differs for negative parity.

TABLE IX. Resonances in ^{163}Dy(n,γ): The energies and spins are from Mughabghab's compilation (Atlas) [10], RPI work [39] and present analysis (DANCE). Only resonances with a firm spin assignment are reported above 402 eV. For details see Sec. III D 2. Electronic version of the table is available in Suppl. Mat. [44].

E_{res} (eV)			J_{res}		
Atlas	RPI	DANCE[a]	Atlas	RPI	DANCE
1.713	–		2	–	2
5.81	–		?	–	(2)
–	–	14.05	–	–	(2)
16.23	16.2		3	3	3
19.65	19.7		3	3	3
35.79	35.8		2	2	2
50.27	50.3		3	3	3
[b]55.85	55.9	55.86	3	3	3
		55.89			2
58.97	59.1		2	2	2
66.11	66.1		3	3	3
[b]72.00	72.0		2	2	2
[b]72.3	-	-	3	-	-
75.48	75.4		2	2	2
78.99	79		2	2	2
86.30	86.3		3	3	3
94.08	94.1		3	3	3
105.88	105.9		3	3	3
107.2	107.2		2	2	2
–	–	113.2	–	–	(3)
[b]120.33	120.4		3	3	3
126.58	126.6		3	3	3
127.46	127.5		3	3	2
135.31	135.4		3	3	3
143.38	143.5		2	2	2
[b]144.97	145		2	2	2
155.02	155.1		2	2	2
163.81	163.9		3	3	3
–	–	169.6	–	–	(3)
177.18	177.2		3	3	3
185.09	185.2		3	3	3
188.95	189		2	2	2
202.90	203		2	2	2
205.26	205.4		3	3	3
213.74	213.8		3	3	3
224.15	223.9		2	2	2
	224.6			3	3
233.54	233.7		3	3	3
250.55	250.7		3	3	3
261.13	261.3		3	3	3
268.01	268.2		3	3	3
274.17	274.4		2	2	2
281.06	281.2		3	3	3
[b]288.85	289.1		2	2	2
296.00	295.9		(2)	2	3
[b]297.77	297.3		2	2	2
	298.1			2	
307.10	–		3	–	2
323.08	323.1		3	3	3
324.55	324.7		3	3	3
326.93	327.2		?	2	2
329.73	329.7		3	2	3

TABLE IX. (*Continued.*)

E_{res} (eV)			J_{res}		
Atlas	RPI	DANCE[a]	Atlas	RPI	DANCE
342.86	343.1		3	3	3
348.32	348.4		2	2	2
368.64	368.8		3	2	3
374.96	375.4		3	3	(3)
382.16	382.4		3	2	(3)
387.01	387.3		3	2	3
390.44	390.6		2	3	2
400.34	400.4		3	2	3
411.08	411.4		2	2	3
429.38	429.6		2	3	2
454.84	455.1		3	3	3
459.21	459.5		(3)	3	3
465.32	465.5		2	3	2
479.10	479.4		3	2	2
483.55	484.0		3	2	3

[a]Resonance energies are rough estimates based on the observed position of maxima.
[b]See discussion in Sec. III D 2.

TABLE X. Resonances in ^{167}Er(n,γ): The energies and spins are from Mughabghab's compilation (Atlas) [10] and present analysis (DANCE). Only firm and tentative spin assignments are presented above 285 eV. For details see Sec. III D 3. Electronic version of the table is available in Suppl. Mat. [44].

E_{res} (eV)		J_{res}	
Atlas	DANCE[a]	Atlas	DANCE
0.460		4	4
0.584		3	3
5.994		3	3
7.93		4	4
9.39		3	3
20.23		4	4
22.02		3	3
26.24[b]		3	3
27.42		4	4
32.89		4	4
37.59		4	4
39.43		3	3
42.23		3	3
50.19		4	4
53.60	53.4	4	3
	53.8		4
59.96		3	3
62.07		4	4
62.78		3	3
69.43		4	4
74.37		4	4
75.77		4	4
79.29		3	3
85.42		3	3
91.2		4	4

TABLE X. (*Continued.*)

E_{res} (eV)		J_{res}	
Atlas	DANCE[a]	Atlas	DANCE
94.8	94.6	4	3
	94.8		4
97.5		4	4
98.2		4	3
107.6		3	3
112.9		4	4
115.6		3	3
128.3		3	(3)
131.6	131.4	4	4
	131.6		3
142.3		4	4
142.9		?	(4)
150.5		4	4
153.18		3	3
157.8		3	3
159.4		4	4
162.2		4	4
165.1		4	4
166.8		3	3
168.5		3	3
176.8		4	4
178.5		4	4
184.7		4	4
191.3		4	4
196.0		3	(3)
204[b]		?	(4)
209.9	209.9	3	3
	210.3		4
217.2		4	4
223.3		3	4
228.7	228.6	3	3
	229.1		4
230.1		?	4
235.5		3	3
237.9		4	4
238.7		?	3
247.3		3	4
249.2	249.1	3	(3)
	249.4		(4)
258.2		4	4
263.3		4	4
274.5		3	3
279.9		3	4
282.5		4	4
297.6		?	(3)
309.5		3	3
327.2		4	(4)
331.6		(4)	(3)
335.1		4	(4)
343.3		4	4
346.5		3	(3)
355.5		?	3
358.1		4	4
363.7		4	4
368.3		4	4

TABLE X. (*Continued.*)

E_{res} (eV)		J_{res}	
Atlas	DANCE[a]	Atlas	DANCE
373.4		?	(4)
381.8		3	3
387.6		3	3
399.6		3	4
408.0		(4)	4
411.7		?	4
418.8		?	(4)
429.0		(3)	3
437.2		3	4
442.2		?	(4)
446.6		3	4
455.8		3	(4)
485.4		4	4
505.9		(4)	4
590.1		4	4
665.98		?	3

[a]Resonance energies are rough estimates based on the observed position of maxima.
[b]See discussion in Sec. III D 3.

multiplicity-based method in combination with the calorimetric capabilities of the detector enabled us to identify new resonances in all three isotopes, some of them being members of close doublets, and to assign (at least tentative) spin to all resonances up to 209, 402, and 285 eV in ^{161}Dy, ^{163}Dy, and ^{167}Er, respectively. In addition, we identified spins of several resonances at higher energies for all three isotopes. Newly reported resonances impact average resonance spacings. Precise information on resonance spins then allows us to check the ratio of spacings for the two spins formed in s-wave resonance capture against predictions of different nuclear level density models—many models available in the literature are consistent with our ratios with the exception of a few microscopical NLD models available in TALYS.

A detailed analysis of completeness of the observed resonance sequences, based both on properties of Porter-Thomas distribution as well as resonance position predictions from GOE, was performed. This analysis showed that it is difficult to unambiguously assess the completeness of the measured resonance sequence and/or to determine precisely the number of missing resonances. It also clearly revealed that sequences consisting of more than a few tens of resonances—about 40–70 for mixed-spin ones—are almost surely incomplete for well-deformed rare-earth odd-mass targets. Despite these restrictions, the high-resolution power of the method for distinguishing close doublets in combination with the analysis of the number of missing resonances allows the determination of s-wave average resonance spacing with an uncertainty of a few percent. We propose $D_0 = 2.15(5)$, 6.39(24), and 3.86(12) eV for ^{161,163}Dy and ^{167}Er, respectively.

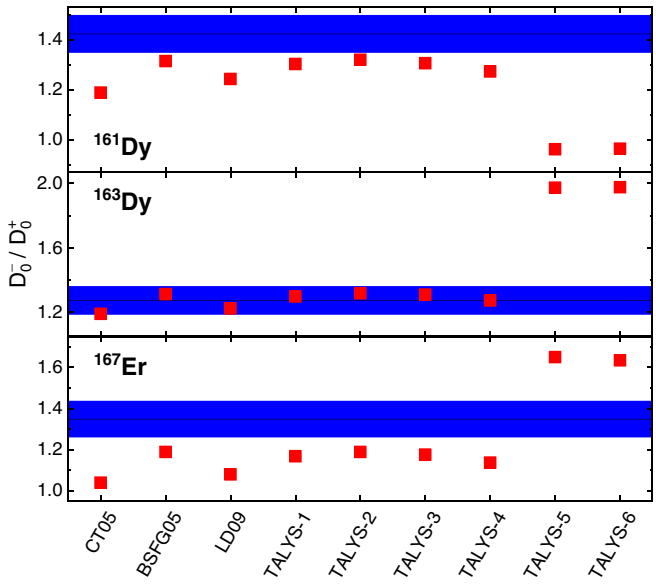

FIG. 10. Comparison of experimental D_0^-/D_0^+ ratio for s-wave resonances with predictions of a few NLD models. The experimental value corresponds to the highest E_{max}, and blue corridor depicts uncertainty of the experimental ratio. The values from LD models of TALYS 1.8 [47], labeled therein as `ldmodel` 1–6 [48], are shown as TALYS-1–TALYS-6. Values labeled CT05 and BSFG05 correspond to constant temperature and back-shifted Fermi gas models from Ref. [49], and label LD09 indicates spin dependence from Ref. [50].

ACKNOWLEDGMENTS

The authors thank F. Bečvář for fruitful discussions and R. Casten for helpful comments as well as for the Er sample. This work was supported by the U. S. Department of Energy Grants No. DE-NA0001784 and No. DE-FG02-97-ER41042, the Grant No. 19-14048S of the Czech Science Foundation, and the Charles University Projects No. UNCE/SCI/013, No. SVV 260576, and No. GAUK 590218. This work benefited from the use of the LANSCE accelerator and was performed under the auspices of the U. S. Department of Energy at Los Alamos National Laboratory by the Los Alamos National Security, LLC under Contract No. DE-AC52-06NA25396.

APPENDIX A: MONTE CARLO RESONANCE SEQUENCES

To study subthreshold resonances, we simulated 10^4 random sequences of resonances within the statistical approach, i.e., using average resonance spacing for given spin and parity, neutron strength functions S_ℓ, resonance positions from GOE, and Porter-Thomas fluctuation of individual reduced neutron widths. Each resonance was randomly assigned $g\Gamma_n$, where g is the statistical factor. One random sequence of s- and p-wave resonances is shown in Fig. 5.

For the comparison of experimental sequences with the RMT predictions, we diagonalized 5000 randomly generated GOE matrices and unfolded the eigenvalues for the Wigner's semicircle law in the same way as in Ref. [51]. The matrices were large enough to get individual sequences of the same length as in the experiment. The average simulated spacing was adjusted consistently with the experiment. For the mixed-spin sequences, we have tested several different reasonable

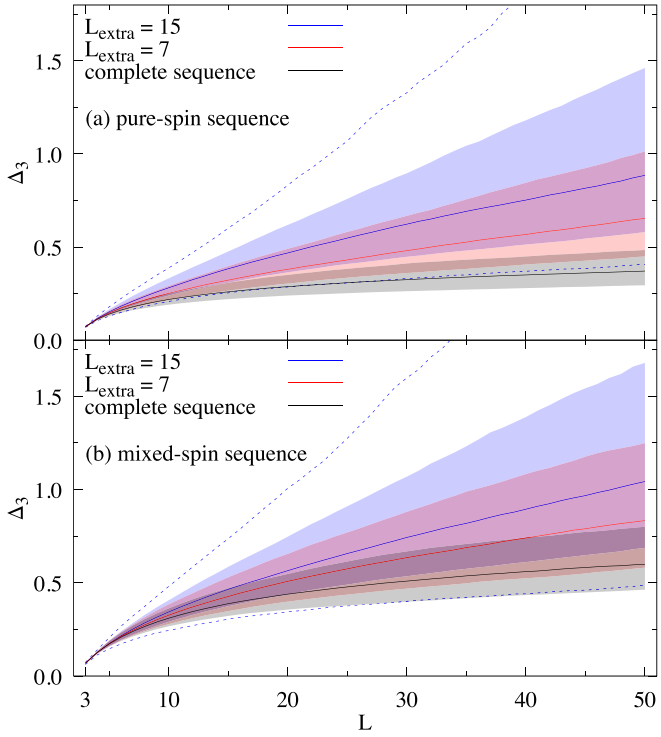

FIG. 11. The simulated Δ_3 statistic as a function of L for sequences with $L_{\max} = 50$ and $L_{\text{extra}} = 0, 7$, and 15 for pure-spin (a) and mixed-spin (b) cases. The shaded corridors correspond to 68.27% central interval and the dashed lines for $L_{\text{extra}} = 15$ show the edges of 95.45% central interval.

values of the mixing parameter, and the results are independent of the exact parameter value.

APPENDIX B: DISCUSSION OF SENSITIVITY OF TESTED STATISTICS

Simulations of incomplete sequences allow not only checking the sensitivity of different statistics to missing resonances but also verifying the possibility to estimate the number of missing resonances using these statistics (as proposed, e.g., for Δ_3 by Mulhall *et al.* [45]). As already indicated by Mitchell and Shriner [52], the sensitivity of various tests based on resonance positions to a single (or a few) missing level is restricted. Our results presented above confirm this fact but we would like to discuss the sensitivity of the tests in more detail here.

To assess the sensitivity of different statistics, we have simulated both pure- and mixed-spin sequences of various lengths. We will focus here on $L_{\max} = 50$ case, as the experimental mixed-spin sequences analyzed in this paper are of similar length. The below presented conclusions hold for values of $L_{\max}$ in the order of tens to two hundred.

In Fig. 11, we plot the $\Delta_3(L)$ for complete sequences and those with ≈15% and 30% of missing resonances, i.e., for $L_{\text{extra}} = 0, 7$, and 15. From the distributions of $\Delta_3(L_{\max})$ values, i.e., from the overlap of central 68.27% intervals in Fig. 11, it is evident that the number of missing resonances

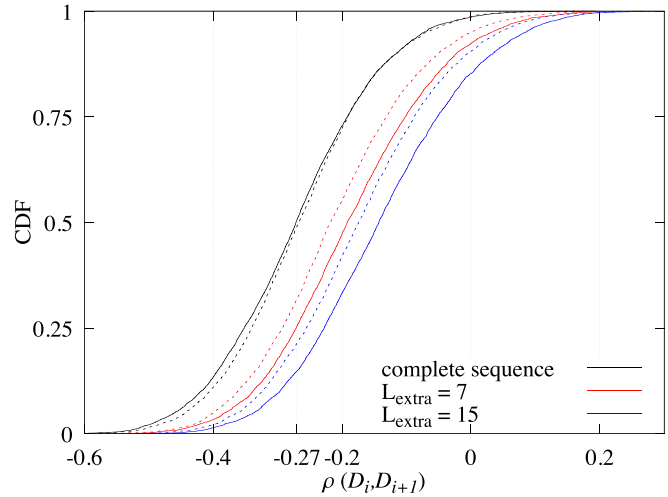

FIG. 12. Cumulative distribution function of the simulated correlation coefficient $\rho(D_i, D_{i+1})$ for pure-spin (solid) and mixed-spin (dashed) sequences of $L_{\max} = 50$. The complete sequences are compared to sequences with ≈15% and 30% of missing resonances, i.e., for $L_{\text{extra}} = 7$ and 15.

should not be estimated based on the value $\Delta_3^{\text{exp}}(L_{\max})$. Even when the hypothesis of completeness is rejected, the experimental $\Delta_3^{\text{exp}}(L_{\max})$ is likely to be compatible with wide range of L_{extra} values. For example, the experimental sequence in Fig. 9(b) is not compatible with the complete one's 68.27% central interval; however, the allowed range of L_{extra} is 1 to 30. Furthermore, for sequences which show a low value of $\Delta_3(L_{\max})$, one can say that the sequence is compatible with hypothesis of completeness, but often also with hypothesis of small L_{extra} even on 68.27% level. The example in Fig. 9(a) showcases compatibility with $L_{\text{extra}} = 0$–3 and 0–18 within 68.27% and 95.45% central intervals, respectively.

As shown in Table III, the allowed number of missed resonances is 0–3 when using more sophisticated criterion for the Δ_3 statistic introduced in Sec. IV B. Because of the highly nontrivial correlation between Δ_3 values for different L, the probability that the whole chain of $\Delta_3(L)$ points for complete sequence stays within 95.45% central interval is ≈80%[4] and ≈76%[4] for pure- and mixed-spin sequences, respectively. On the other hand, the probability that a $L_{\text{extra}} = 7$ sequence is not rejected as a complete one is ≈58% and ≈85% for pure- and mixed-spin cases; these probabilities decrease to ≈27% and ≈69% for $L_{\text{extra}} = 15$.

The cumulative distribution function of simulated correlation coefficient is shown in Fig. 12 for pure- and mixed-spin sequences with $L_{\max} = 50$ and 0, ≈15%, and 30% of missing resonances. While we observe a shift (and widening) of the distribution with increasing L_{extra}, it is not large enough to provide significant sensitivity in general. The fact that we observe some sensitivity, as presented in Tables III–V, is given

[4]Compare this to a probability that 50 randomly drawn values from Normal distribution are *all* within $\pm 2\sigma$, which is ≈10%.

by the extreme values of experimental correlation coefficients, e.g., $\rho^{\exp} = -0.6164$ and -0.0323 for ^{167}Er sequence of 3^+ resonances up to 200 eV and ^{161}Dy mixed-spin sequence up to 209 eV, respectively. Analogous behavior is observed for the NNSD. An illustration of changes in the cumulative distribution of NNSD is for a few values of L_{extra} shown in Fig. 7.

[1] M. Arnould and S. Goriely, Prog. Part. Nucl. Phys. **112**, 103766 (2020).

[2] J. J. Cowan, C. Sneden, J. E. Lawler, A. Aprahamian, M. Wiescher, K. Langanke, G. Martínez-Pinedo, and F.-K. Thielemann, Rev. Mod. Phys. **93**, 015002 (2021).

[3] Report of the Nuclear Physics and Related Computational Science R&D, in *Advanced Fuel Cycles Workshop* (Bethesda, MD, 2006).

[4] F. Bečvář, P. Koehler, M. Krtička, G. Mitchell, and J. Ullmann, Nucl. Instrum. Methods Phys. Res., Sect. A **647**, 73 (2011).

[5] F. J. Dyson and M. L. Mehta, J. Math. Phys. **4**, 701 (1963).

[6] C. E. Porter, *Statistical Theories of Spectra: Fluctuations; a Collection of Reprints and Original Papers, with an Introductory Review*, Perspectives in Physics (Academic Press, San Diego, 1965).

[7] H. I. Liou, H. S. Camarda, S. Wynchank, M. Slagowitz, G. Hacken, F. Rahn, and J. Rainwater, Phys. Rev. C **5**, 974 (1972).

[8] D. Mulhall, Phys. Rev. C **80**, 034612 (2009); Erratum in Ref. [53].

[9] U. Agvaanluvsan Jr., G. E. Mitchell, J. F. Shriner, and M. P. Pato, Nucl. Instrum. Methods Phys. Res., Sect. A **498**, 459 (2003).

[10] S. F. Mughabghab, *Atlas of Neutron Resonances* (Elsevier, Amsterdam, 2018), Vol. 2.

[11] P. W. Lisowski, C. D. Bowman, G. J. Russell, and S. A. Wender, Nucl. Sci. Eng. **106**, 208 (1990).

[12] M. Heil, R. Reifarth, M. M. Fowler, R. C. Haight, F. Käppeler, R. S. Rundberg, E. H. Seabury, J. L. Ullmann, and K. Wisshak, Nucl. Instrum. Methods Phys. Res., Sect. A **459**, 229 (2001).

[13] R. Reifarth, T. A. Bredeweg, A. Alpizar-Vicente, J. C. Browne, E.-I. Esch, U. Greife, R. C. Haight, R. Hatarik, A. Kronenberg, J. M. O'Donnell, R. S. Rundberg, J. L. Ullmann, D. J. Vieira, J. B. Wilhelmy, and J. M. Wouters, Nucl. Instrum. Methods Phys. Res., Sect. A **531**, 530 (2004).

[14] M. Jandel, T. A. Bredeweg, A. J. Couture, M. M. Fowler, E. M. Bond, M. B. Chadwick, R. R. C. Clement, E.-I. Esch, J. M. O'Donnell, R. Reifarth, R. S. Rundberg, J. L. Ullmann, D. J. Vieira, J. B. Wilhelmy, J. M. Wouters, R. A. Macri, C. Y. Wu, and J. A. Becker, Nucl. Instrum. Methods Phys. Res., Sect. B **261**, 1117 (2007).

[15] J. M. Wouters, A. Alpizar-Vicente, T. A. Bredeweg, E.-I. Esch, R. C. Haight, R. Hatarik, J. M. O'Donnell, R. Reifarth, R. S. Rundberg, J. M. Schwantes, S. A. Sheets, J. L. Ullmann, D. J. Vieira, and J. B. Wilhelmy, IEEE Trans. Nucl. Sci. **53**, 880 (2006).

[16] S. Mosby, A. J. Couture, M. Jandel, and J. M. O'Donnell, Los Alamos National Laboratory Report No. LA-UR-18-22130, 2018 (unpublished).

[17] S. Valenta, B. Baramsai, T. A. Bredeweg, A. J. Couture, A. Chyzh, M. Jandel, J. Kroll, M. Krtička, G. E. Mitchell, J. M. O'Donnell, G. Rusev, J. L. Ullmann, and C. L. Walker, Phys. Rev. C **96**, 054315 (2017).

[18] P. Schillebeeckx, B. Becker, Y. Danon, K. Guber, H. Harada, J. Heyse, A. R. Junghans, S. Kopecky, C. Massimi, M. C. Moxon, N. Otuka, I. Sirakov, and K. Volev, Nucl. Data Sheets **113**, 3054 (2012).

[19] D. J. Horen, J. A. Harvey, and N. W. Hill, Phys. Rev. C **24**, 1961 (1981).

[20] C. Massimi, A. Borella, S. Kopecky, C. Lampoudis, M. Moxon, P. Schillebeeckx, and G. Vannini, Nuovo Cimmento B **125**, 517 (2010).

[21] E. Reddingius, H. Postma, C. E. Olsen, D. C. Rorer, and V. L. Sailor, Nucl. Phys. A **218**, 84 (1974).

[22] G. Brunhart and V. L. Sailor, Phys. Rev. C **2**, 1137 (1970).

[23] C. Coceva, F. Corvi, P. Giacobbe, and G. Carraro, Nucl. Phys. A **117**, 586 (1968).

[24] K. J. Wetzel and G. E. Thomas, Phys. Rev. C **1**, 1501 (1970).

[25] S. Kahane, S. Raman, G. G. Slaughter, C. Coceva, and M. Stefanon, Phys. Rev. C **30**, 807 (1984).

[26] P. E. Koehler, A. C. Larsen, M. Guttormsen, S. Siem, and K. H. Guber, Phys. Rev. C **88**, 041305(R) (2013).

[27] S. A. Sheets, U. Agvaanluvsan, J. A. Becker, F. Bečvář, T. A. Bredeweg, R. C. Haight, M. Krtička, M. Jandel, G. E. Mitchell, J. M. O'Donnell, W. E. Parker, R. Reifarth, R. S. Rundberg, E. I. Sharapov, I. Tomandl, J. L. Ullmann, D. J. Vieira, J. M. Wouters, J. B. Wilhelmy, and C. Y. Wu, Phys. Rev. C **76**, 064317 (2007).

[28] P. E. Koehler, J. L. Ullmann, T. A. Bredeweg, J. M. O'Donnell, R. Reifarth, R. S. Rundberg, D. J. Vieira, and J. M. Wouters, Phys. Rev. C **76**, 025804 (2007).

[29] F. Gunsing, K. Fraval, M. Mathelie, S. Valenta, F. Bečvář, G. Rusev, A. P. Tonchev, G. Mitchell, B. Baramsai, S. Altstadt *et al.* (n_TOF Collaboration), Nucl. Data Sheets **119**, 132 (2014).

[30] C. E. Porter and R. G. Thomas, Phys. Rev. **104**, 483 (1956).

[31] F. Bečvář, Nucl. Instrum. Methods Phys. Res., Sect. A **417**, 434 (1998), Erratum in Ref. [54].

[32] M. Krtička and S. Valenta, https://www-nds.iaea.org/dicebox/

[33] C. M. Baglin, Nucl. Data Sheets **111**, 1807 (2010).

[34] C. W. Reich, Nucl. Data Sheets **108**, 1807 (2007).

[35] B. Singh and J. Chen, Nucl. Data Sheets **147**, 1 (2018).

[36] B. Baramsai, J. Kroll, G. E. Mitchell, U. Agvaanluvsan, F. Bečvář, T. A. Bredeweg, A. Chyzh, A. Couture, D. Dashdorj, R. C. Haight, M. Jandel, A. L. Keksis, M. Krtička, J. M. O'Donnell, R. S. Rundberg, J. L. Ullmann, D. J. Vieira, and C. L. Walker, Phys. Rev. C **87**, 044609 (2013).

[37] A. Chyzh, B. Baramsai, J. A. Becker, F. Bečvář, T. A. Bredeweg, A. Couture, D. Dashdorj, R. C. Haight, M. Jandel, J. Kroll, M. Krtička, G. E. Mitchell, J. M. O'Donnell, W. Parker, R. S. Rundberg, J. L. Ullmann, D. J. Vieira, C. L. Walker, J. B. Wilhelmy, J. M. Wouters *et al.*, Phys. Rev. C **84**, 014306 (2011).

[38] S. Agostinelli *et al.*, Nucl. Instrum. Methods Phys. Res., Sect. A **506**, 250 (2003).

[39] S. G. Shin, Y. U. Kye, W. Namkung, M. H. Cho, Y.-R. Kang, M. W. Lee, G. N. Kim, T.-I. Ro, Y. Danon, D. Williams, G. Leinweber, R. C. Block, D. P. Barry, and M. J. Rapp, Eur. Phys. J. A **53**, 203 (2017).

[40] S. G. Shin, Y. U. Kye, W. Namkung, M. H. Cho, Y.-R. Kang, M. W. Lee, G. N. Kim, T.-I. Ro, J. E. Lee, T. Katabuchi, and K. Terada, Eur. Phys. J. A **54**, 226 (2018).

[41] H. I. Liou, G. Hacken, J. Rainwater, and U. N. Singh, Phys. Rev. C **11**, 462 (1975).

[42] E. P. Wigner, Oak Ridge Nat. Lab. Report No. ORNL-2309, 1957, https://technicalreports.ornl.gov/1957/3445602508212.pdf.
[43] J. Zhang, J. R. Statist. Soc. B **64**, 281 (2002).
[44] See Supplemental Material at http://link.aps.org/supplemental/10.1103/PhysRevC.106.034607 for electronic versions of the tables.
[45] D. Mulhall, Z. Huard, and V. Zelevinsky, Phys. Rev. C **76**, 064611 (2007).
[46] R. Capote, M. Herman, P. Oblozinsky, P. C. Young, S. Goriely, T. Belgya, A. V. Ignatyuk, A. J. Koning, S. Hilaire, V. A. Plujko, M. Avrigeanu, O. Bersillon, M. B. Chadwick, T. Fukahori, Z. Ge, Y. Han, S. Kailas, J. Kopecky, V. M. Maslov, G. Reffo *et al.*, Nucl. Data Sheets **110**, 3107 (2009).
[47] A. J. Koning, S. Hilaire, and M. C. Duijvestijn, in *International Conference on Nuclear Data for Science and Technology*, edited by O. Bersillon, F. Gunsing, E. Bauge, R. Jacqmin, and S. Leray (CEA; OECD Nucl. Energy Agency, EDP Sciences, Les Ulis, France, 2008), pp. 211–214.
[48] A. J. Koning, S. Hilaire, and S. Goriely, TALYS, https://tendl.web.psi.ch/tendl_2019/talys.html.
[49] T. von Egidy and D. Bucurescu, Phys. Rev. C **72**, 044311 (2005); **73**, 049901(E) (2006).
[50] T. von Egidy and D. Bucurescu, Phys. Rev. C **80**, 054310 (2009).
[51] P. E. Koehler, F. Bečvář, M. Krtička, K. H. Guber, and J. L. Ullmann, Fortschr. Phys. **61**, 80 (2013).
[52] G. E. Mitchell and J. F. Shriner Jr., International Atomic Energy Agency Report No. INDC(NDS)-0561, Vienna, 2009, https://www-nds.iaea.org/missing-levels/indc-nds-0561.pdf.
[53] D. Mulhall, Phys. Rev. C **82**, 029904(E) (2010).
[54] F. Bečvář, Nucl. Instrum. Methods Phys. Res., Sect. A **935**, 240 (2019).